Journal of Alloys and Compounds 509 (2011) 6711–6719

Contents lists available at ScienceDirect

Journal of Alloys and Compounds

journal homepage: www.elsevier.com/locate/jallcom

High-quality vertically aligned ZnO nanorods synthesized by microwave-assisted CBD with ZnO–PVA complex seed layer on Si substrates

J.J. Hassan*, Z. Hassan, H. Abu-Hassan

Nano-Optoelectronics Research and Technology Laboratory (N.O.R), School of Physics University Sains Malaysia, Penang 11800, Malaysia

ARTICLE INFO

Article history:
Received 13 December 2010
Received in revised form 23 March 2011
Accepted 28 March 2011
Available online 5 April 2011

Keywords:
ZnO
Nanorods
PVA–ZnO nanocomposites seed
Microwave assisted
Chemical bath deposition
FESEM
Photoluminescence
Raman

ABSTRACT

We successfully synthesized vertically aligned zinc oxide (ZnO) nanorods on seeded silicon substrates using chemical bath deposition assisted by microwave heating. ZnO nanorods were grown on seed layers of ZnO–polyvinyl alcohol (PVA) nanocomposites spin-coated on p-type Si (1 1 1). The nanorod's diameter was found to be dependent on the annealing temperature of the ZnO–PVA seed layer. We produced ZnO nanorods with diameters in the range of 50–300 nm from five groups of seed layers annealed at 250 °C, 350 °C, 380 °C, 450 °C, and 550 °C. The nanorods were examined with X-ray diffraction, transmission electron microscopy, and field emission scanning electron microscopy, which revealed hexagonal wurtzite structures perpendicular to the substrate along the z-axis in the direction of (0 0 2). Photoluminescence measurements revealed high UV emission at a high I_{UV}/I_{vis} ratio of 175. We also conducted Raman scattering studies on the ZnO nanorods to estimate the lattice vibration modes.

1. Introduction

One-dimensional semiconductor nanorod/nanowire structures have been widely used recently because of their special properties of quantum confinement, high surface-to-volume ratio, higher optical gain, faster response, and specific crystalline orientation [1,2]. The quantum confinement of these structures is related to electronic quantum transport and enhanced radiative recombination of carriers [3]. Zinc oxide (ZnO), a wide bandgap (3.37 eV) semiconductor with a high exciton binding energy of 60 meV, and large internal piezoelectric coefficient, is a potentially significant and functional material for nanorod/nanowire structures [4]. ZnO nanorod/nanowire structures can be used as foundation blocks in a variety of applications such as short-wavelength nanolasers [5,6], field-effect transistors [7], nanosized gas sensors [8–10], nanoresonators, UV sensors [11–13], nanocantilevers [14], blue electroluminescent devices [15], high heterojunction area solar cells [16–18], and field emitters [19]. ZnO nanorods/nanowires can be grown using a variety of methods such as chemical vapor deposition (CVD), thermal evaporation [20,21], electrodeposition [22,23], catalyst-free combust-oxidized mesh (CFCOM) [24], oxidizing in air Zn metal films [25], and chemical bath deposition (CBD) [26–28]. Among these methods, CBD is a flexible technique to synthesis ZnO nanostrucures with a powerfully controlling on their morphology. A variety of ZnO nanostructures such as nanorods, nanowires, nanotubes and nanobelts, etc. were synthesized on different substrates applying this method. Depending on the synthesis parameters such as temperature, substrate type, seeding layer, deposition time, and solvent used, the structure and the orientation can be effectively controlled [25].

Vertically aligned ZnO nanorods grown on a variety of substrates such as transparent conducting oxide, silicon, ceramic [29], and GaN on sapphire [30], have attracted attention for applications such as electroluminescent devices and light-emitting diodes [31,32]. Functional nanodevice assembly requires controlled growth of nanorods to achieve desired size and density. Reports on the synthesis of ZnO nanorods by CBD have used various ZnO seed layers as nucleation sites for the growth of the ZnO nanorods [33–35]. Sang et al. [36] synthesized ZnO nanorods using high purity N_2 as a carrier gas which carried Zn vapor obtained by the pyrolysis of $Zn(CH_3COO)_2{\cdot}2H_2O$ and pass through silicon substrate seeded with PVA–ZnO nanocomposites placed in specialized furnace. Kumar et al. [37] used successive ionic layer adsorption and reaction (SILAR) to prepare ZnO seed layer on a silicon substrate and then grew ZnO nanorods using the CBD method. Tao et al. [38] and Kenannkis et al. [39] used thin film of ZnO deposited by RF sputtering and via the sol–gel/spin coating technique to synthesize ZnO nanorods on silicon substrate by CBD. Kang et al. [40] synthesized high quality ZnO nanorods by the combining hydrothermal and CVD methods. Yang et al. [41] described the facile solvothermal

* Corresponding author. Tel.: +60 174497314; fax: +60 46579150.
E-mail address: j1j2h72@yahoo.com (J.J. Hassan).

0925-8388/$ – see front matter © 2011 Elsevier B.V. All rights reserved.
doi:10.1016/j.jallcom.2011.03.153

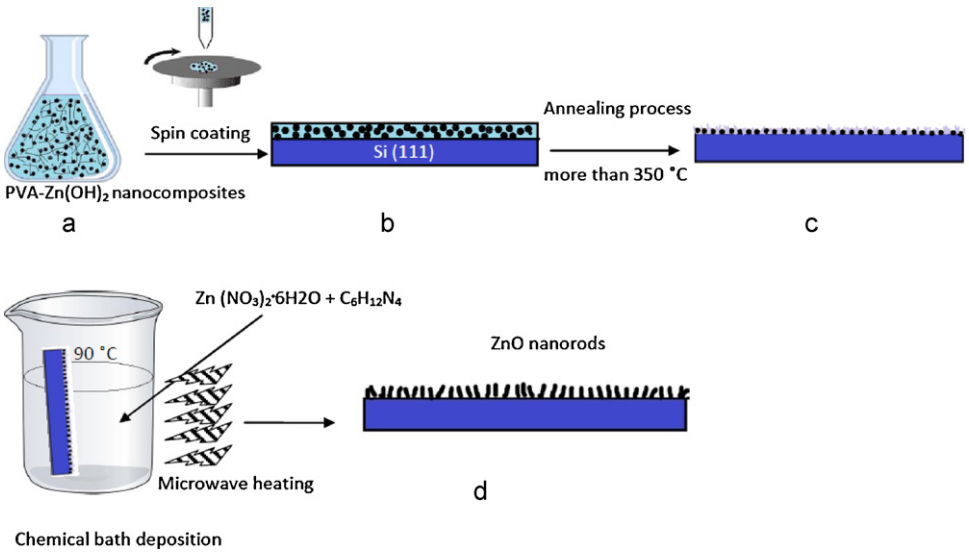

Fig. 1. ZnO nanorods growth mechanism diagram.

approach to synthesize various ZnO microstructures by adjusting several controllable parameters such as temperature, concentration, and time. However, nothing in the literature addresses the use of ZnO–PVA as a seed layer on silicon substrates in microwave-assisted CBD. The major role of PVA polymer is the formation of carbon backbone grids after carbonizing the ZnO–PVA seed layer, which limits the growth of ZnO nanorods within these grids. In this study, we use nanocomposites ZnO–PVA as a seed layer to grow ZnO nanorods on silicon (1 1 1) substrates. Microwave heating with CBD superheats the reaction vessel with a homogenous distribution of temperature across the entire vessel. Accordingly, our system consists of superheating ZnO nanocrystal seeds and PVA carbon grids to synthesize vertically aligned ZnO nanorods/nanowires with a large substrate area.

2. Experimental

All chemicals used were analytical grade without further purification. The synthesis of ZnO nanorods consisted of two steps.

The first step was the preparation of the ZnO–PVA seed layer. To prepare the seed layer, we used the procedure described by He et al. [42] with several modifications. In this method, 0.1 mol/L of zinc chloride was dissolved in deionized (DI) water at 70 °C and vigorously stirred for 10 min. Similarly, 1.5 g of PVA was dissolved in 50 mL DI water at 80 °C stirred for 30 min. The solutions were mixed together via high-speed stirring and placed on a hot plate at 70 °C for 2 h. The solution was transferred to a microwave oven for 15 min at 80 °C to facilitate complexation of zinc with PVA. At that stage, the pH of the solution was 4.0. To create the $Zn(OH)_2$ complex with PVA polymer chains, ammonia solution was added to the mixture until the pH reached 8.3 and the solution became milky white. The PVA–$Zn(OH)_2$ complex solution was then spin-coated on a silicon substrate {p-type, (1 1 1)} etched with 1:20 HF:DI water for 60 s; this spin-coating process was repeated ten times. Between each coating cycle, the substrate was placed on a hot plate at 150 °C for 2 min. After spin coating, the substrate was placed on a hot plate at 210 °C for 1 h to form ZnO and to decompose the PVA chain and create carbon backbone grids [36]. Five set of substrates were annealed at different temperatures ranging from 250 °C to 550 °C, after which the substrates were ready for use.

The second step was the growth of ZnO nanorods. First, 0.1 mol/L of zinc nitrate hexahydrate $Zn(NO_3)_2{\cdot}6H_2O$ was dissolved in DI water at 70 °C, and an equal molar concentration of hexamethylenetetramine ($C_6H_{12}N_4$) was dissolved in DI water at 70 °C. The two solutions were then mixed in a beaker containing the ZnO–PVA seed layer coated on silicon substrates. The substrates were inclined at 80° in the beaker and then placed inside a microwave oven for 2 h at 90 °C. After complete growth of the ZnO nanorods, the substrates were first washed with hot DI water and then with hot ethanol to remove the remaining salt. They were then dried with nitrogen gas. Finally, the substrates were heated at 550 °C for 1 h in an oxygen flow (5 cm^3/min).

Field emission scanning electron microscopy (FESEM) and energy dispersive X-ray fluorescence spectroscopy (EDX) (model Leo-Supra 50VP, Carl Zeiss, Germany) determined the surface morphology and composition of the ZnO nanorods. Transmission electron microscopy (TEM, model Philips CM12, FEI, CO, The Netherlands) and X-ray diffraction (XRD) (PANalytical X'Pert PRO MRD PW3040, Almelo, The Netherlands) determined their structure and orientation. The optical properties were measured at room temperature by photoluminescence and Raman spectroscopy (Jobin Yvon HR 800 UV, Edison, NJ, USA).

3. Results and discussion

3.1. Growth mechanism of ZnO nanorods

The growth of ZnO nanorods in this study consisted of two steps as described in Fig. 1. The first step was the preparation of the seed layer from the synthesized nanocomposites PVA–$Zn(OH)_2$ (Fig. 1a).

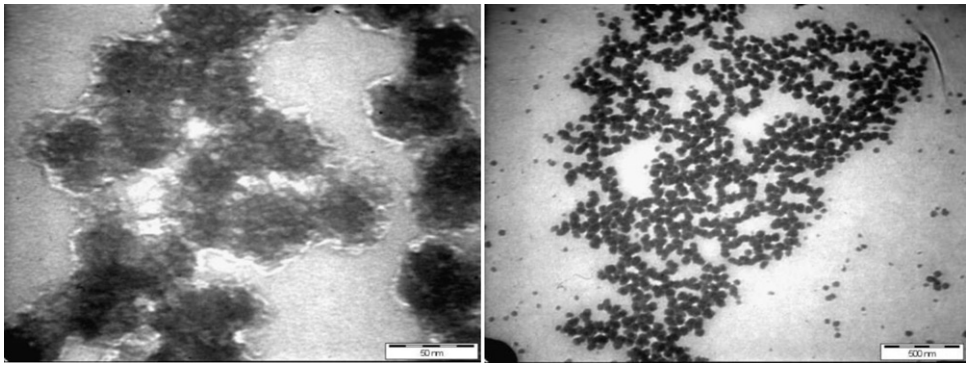

Fig. 2. TEM images of PVA–Zn $(OH)_2$ nanocomposites.

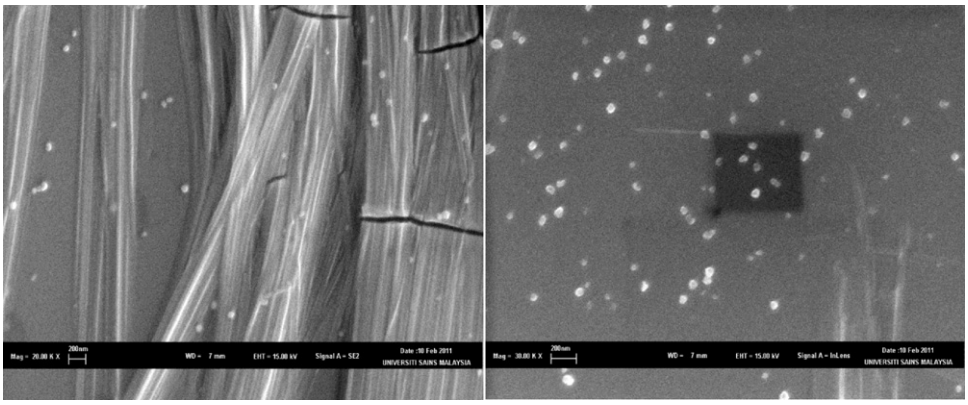

Fig. 3. FESEM images of ZnO–PVA seed layer after spin coated on silicon substrate and annealed at 250 °C for 1 h.

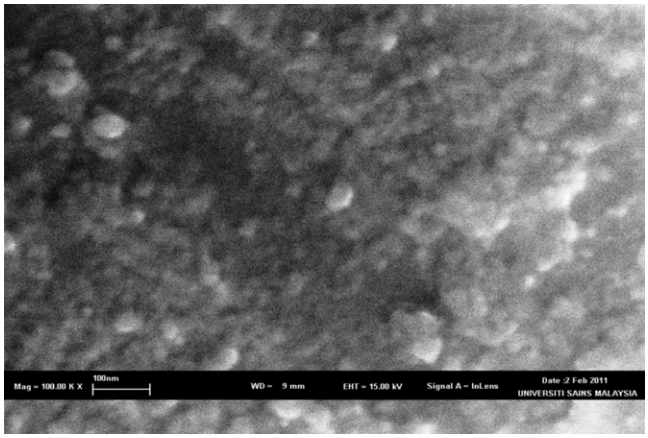

Fig. 4. FESEM images of ZnO–PVA seed layer after spin coated on silicon substrate and annealed at 380 °C for 1 h.

The TEM images in Fig. 2 clearly show the formation of $Zn(OH)_2$ nanoparticles in the range of 50 nm, which are connected with the hydroxyl group of polymer chains according to the following reactions [36]:

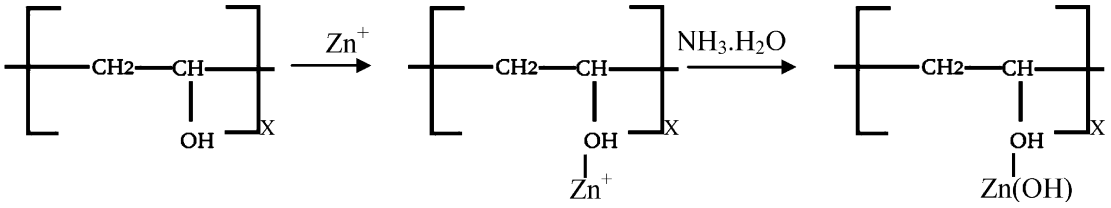

The next stage involved the deposition of the nanocomposites on the silicon substrate using spin-coating techniques. At that stage, the nanoparticles were uniformly distributed within the PVA layer on the Si substrate (Fig. 1b) and did not come in contact with the Si substrate. After the annealing process at 250 °C for 1 h, all $Zn(OH)_2$ nanoparticles decomposed into ZnO nanoparticles as seen in the FESEM images of Fig. 3. When the temperature increased to more than 350 °C (Fig. 1c), the nanoparticles were deposited on the surface of the Si substrate with an accompanying confinement of PVA carbon grids, as clearly seen in the FESEM image of Fig. 4. As a result, the ZnO nanoparticles form a good seed layer on the Si substrate, ready for the next step of ZnO nanorods growth.

The second step used CBD to grow ZnO nanorods on a seed layer (Fig. 1d) that had been prepared in the first step. The growth of ZnO nanorods underwent a process of hydrolysis and condensation of precursors. At that stage, the reaction vessel containing the aqueous solution of zinc nitrite dehydrates as a source of zinc cations and hexamethylenetetramine complex ($C_6H_{12}N_4$) as a slow release of OH^- anions. In that state, the typical reactions were according to the following equations [43]:

$$C_6H_{12}N_4 + 6H_2O \rightarrow 6HCHO + 4NH_3 \quad (1)$$

$$NH_3 + H_2O \rightarrow NH_4^+ + OH^- \quad (2)$$

$$2OH^- + Zn^{2+} \rightarrow Zn(OH)_2 \quad (3)$$

$$Zn(NO_3)_2 \rightarrow Zn^{2+} + 2NO_3^- \quad (4)$$

$$Zn(OH)_2 \xrightarrow{\Delta} ZnO + H_2O \quad (5)$$

The morphology of ZnO in the reaction depended on the hydrolysis and condensation steps of the precursors. Control of the kinetics of the reaction was achieved by introducing controlled amounts of OH^- anions into the solution by a thermal decomposition of hexamethylenetetramine complex. Meanwhile, with the presence of the ZnO seed layer in the solution, the nucleation process occurred quickly. This is a typical effect and is due to a decrease in the activation energy between the zinc oxide crystals and the substrate [44] .The orientation of ZnO rods was significantly dependent on the ZnO seed layer and related to the ZnO wurtzite structure. As a result of the ZnO wurtzite structure, the growth rate of planes followed the following sequence: $(0\ 0\ 0\ 1) > (0\ 1\ \bar{1}\ 0) > (0\ 0\ 0\ \bar{1})$ and this led to the growth of hexagonal rods normal to the substrate in the direction of *c*-axis [45,46].

3.2. XRD analysis

X-ray diffraction patterns of the ZnO nanorods grown on the ZnO–PVA seed layers (on silicon substrates) annealed at different temperatures, ranging from 250 °C to 550 °C and are shown in Fig. 5. The X-ray diffraction patterns match the wurtzite hexagonal phase of ZnO. All the peaks correspond to the ZnO phase, except for the two peaks at 44.5° and 64.4°, which are related to the silicon carbide of the XRD sample holder. Fig. 5(a and b) shows the X-ray diffraction patterns of the ZnO nanorods grown on seeded substrates annealed at 250 °C and 350 °C, respectively. These patterns reveal that the ZnO nanorods were randomly oriented on the substrates, as seen in the FESEM images (Fig. 6(a and b)). Fig. 5c for sample C exhibits

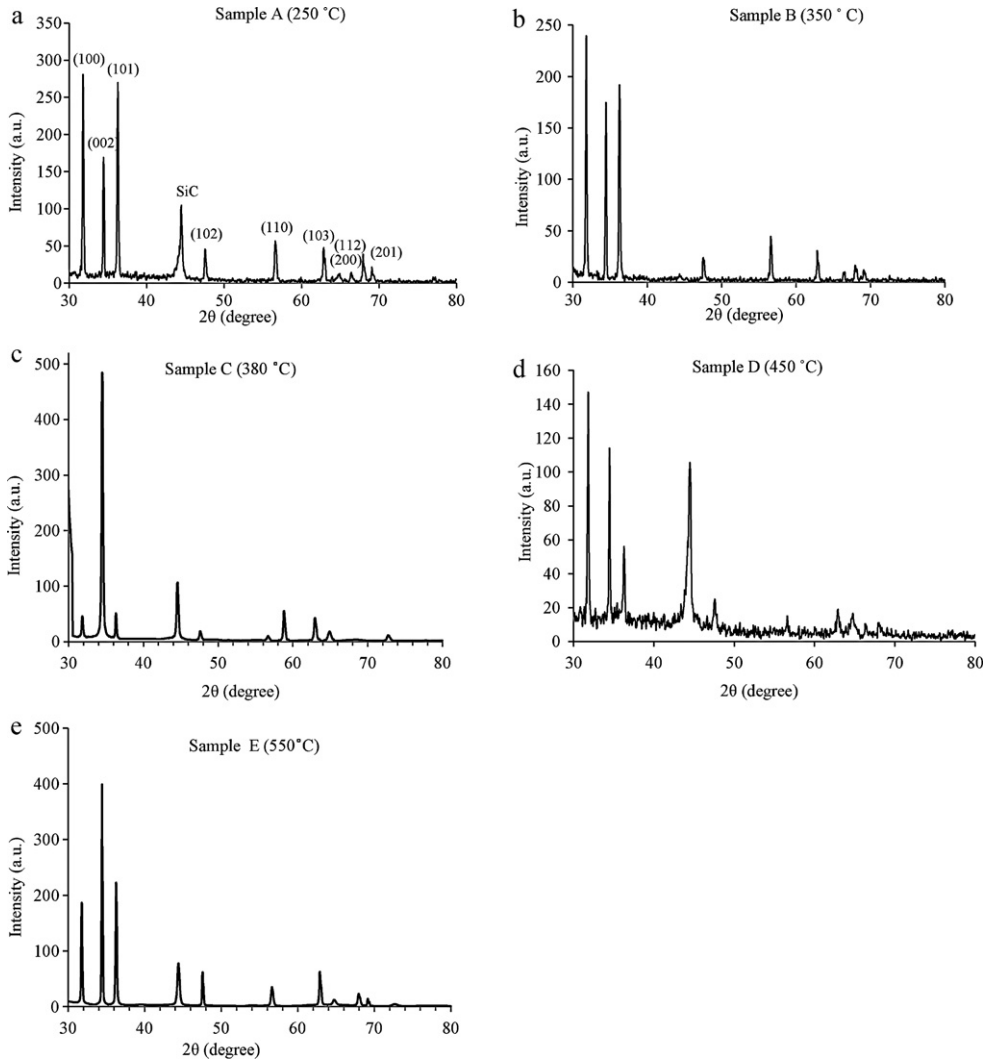

Fig. 5. XRD patterns of ZnO nanorods grown on ZnO–PVA seed layer (on silicon substrate). The seed layers are thermal annealed for one hour at: (a) 250 °C, (b) 350 °C, (c) 380 °C, (d) 450 °C, (e) 550 °C.

strong diffraction in the direction of the *c*-axis (0 0 2), with very weak diffractions from other surfaces. These weak peaks appear due to diffractions from the nanorods grown on the surface (as seen in FESEM image (Fig. 6c)). This confirms the improved alignment of the nanorods grown vertically on the substrate, compared with those in Fig. 5(d and e) for samples D and E, respectively. The strain of the nanorods grown on the silicon substrate along the *c*-axis can be calculated using the following relation [47]:

$$\varepsilon_{ZZ} = \frac{c - c_o}{c_o} \times 100 \quad (6)$$

where c represents the lattice constant of the ZnO nanorods estimated from XRD data and c_o is the standard lattice constant for unstrained ZnO (ICCD 04-006-1673). The strains for samples A–E were 0.0307%, 0.0729%, −0.026%, −0.042%, and −0.09%, respectively; The positive values of samples A and B were associated with the tensile strain while the negative values for the samples C–E revealed the compressive strain for ZnO nanorods. These very low values of tensile and compressive strains suggest that the synthesized ZnO nanorods have a high quality crystal geometry.

3.3. FESEM observation

Fig. 6 shows the FESEM images of nanorods and nanowires prepared by CBD on p-type Si (1 1 1) substrates, with seed layers annealed at different temperatures. Fig. 6(a and b) shows the ZnO nanorods grown on seeded silicon substrate that was annealed at 250 °C for 1 h. It was observed that the nucleation of ZnO rods occurred on the surface of the seed layer and the orientation of the rods was random. This may be due to an uncarbonated seed layer and the polymer covering the ZnO nanocrystal. Also in Fig. 6(c and d) for sample B that was annealed at 350 °C, it can be seen that the ZnO nanorods started to penetrate into the polymer; this was due to the partial carbonization of the polymer. In addition, Fig. 6(e and f) shows the vertically aligned ZnO nanorods rods along the *c*-axis with a high distribution density of rods over the entire sample for sample C in which the seed layer was annealed at 380 °C for 1 h. The low annealing temperature of the ZnO–PVA seed layer (380 °C) may did not decarbonize or destroy the PVA backbone chain carbon grids; thus, the ZnO nanocrystal seed sites were confined by the carbon grids that prevented them from growing to large diameters, which is consistent with the conclusions of Refs. [36,42]. This lead to the growth of small diameter nanorods (60–80 nm) with the CBD technique. A similar situation occurred, as shown in Fig. 6(g and h) for sample D, (seed layer annealed at 450 °C), but the nanorods were not well aligned vertically compared with sample C. This may be due to partial decarburization or distortion of the PVA carbon grids. In that case, the diameter of the ZnO nanorods ranged from 100 nm to 120 nm. Finally, when the annealing temperature of the PVA–ZnO seed layer reached 550 °C

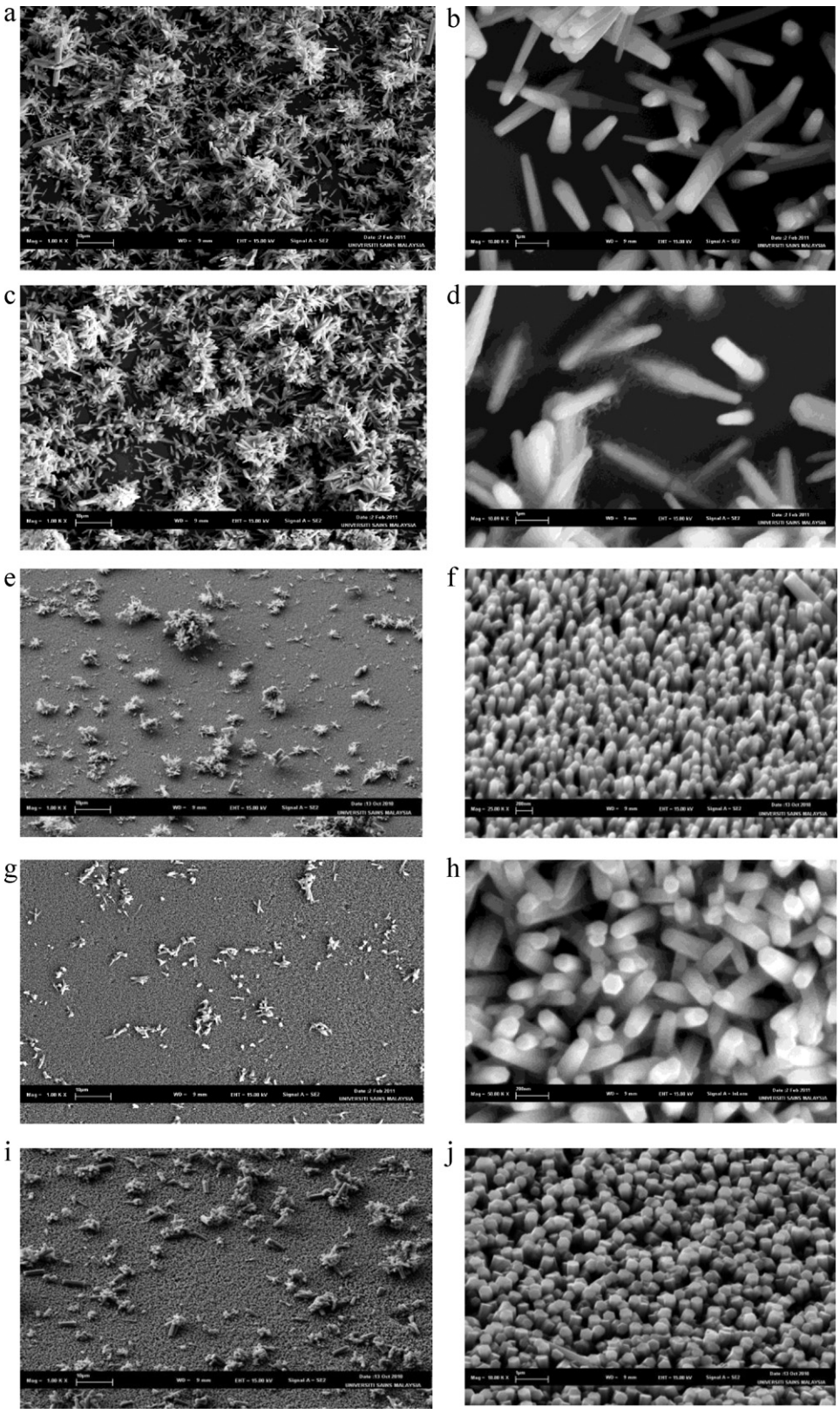

Fig. 6. FESEM images of ZnO nanorods grown on seeded silicon substrates, the annealing temperatures of seed substrates were: (a) and (b) 250 °C, (c) and (d) 350 °C, (e) and (f) 380 °C, (g) and (h) 450 °C, (i) and (j) 550 °C.

(sample E), the carbon grids will reacted with oxygen to form CO_2 gas (decarbonization), and left the ZnO nanoparticles alone without confinement [42]. These nanocrystals grew up on the silicon substrate to form large seed sites, producing wide-diameter ZnO nanorods (200–300 nm), as seen in Fig. 6(i and j). It is clearly shown that the seed layer annealing temperatures exerted a strong influence on the produced nanostructures, as observed on the FESEM images.

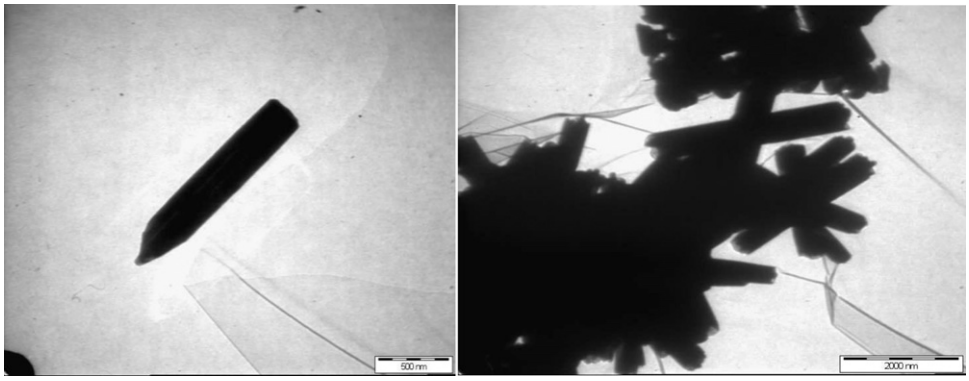

Fig. 7. Typical TEM images of ZnO nanorods at the bottom of the synthesis beaker.

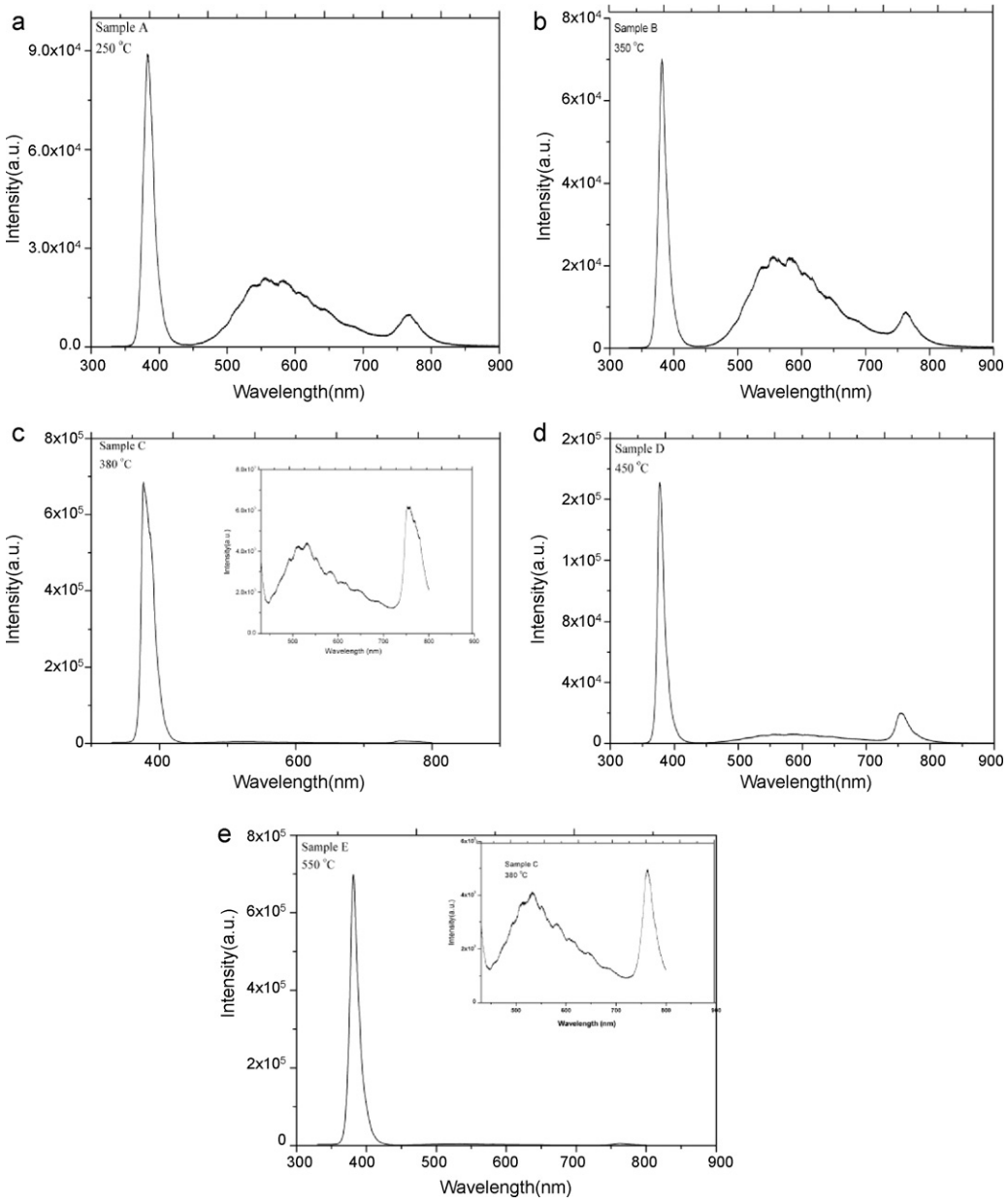

Fig. 8. room temperature photoluminescence for ZnO nanorods grown on silicon substrates seeded with PVA–ZnO nanocomposites, these seeded substrates are annealed at (a) 250 °C, (b) 350 °C, (c) 380 °C, (d) 450 °C, and (e) 550 °C.

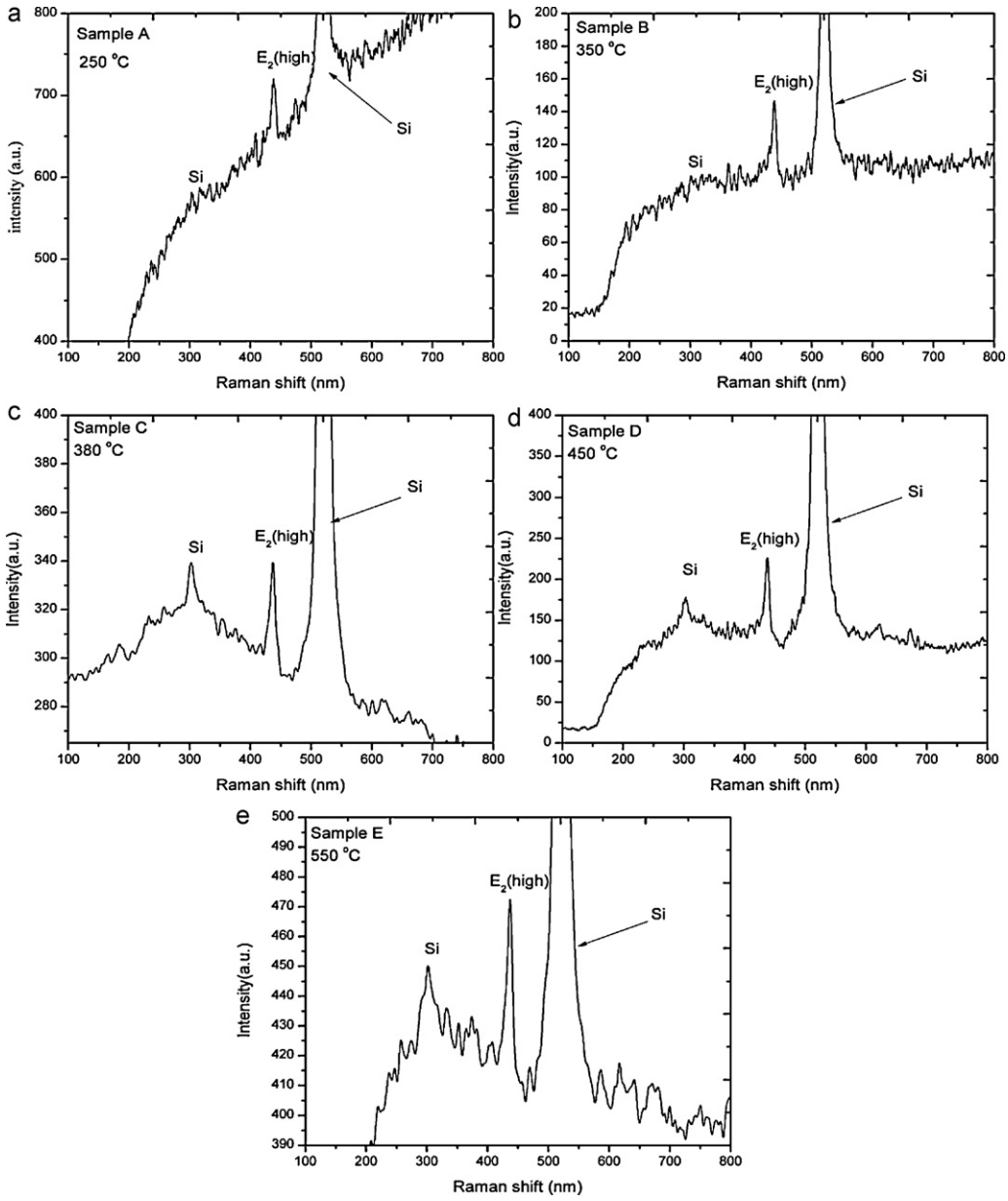

Fig. 9. Raman spectra of ZnO nanorods grown on silicon substrates seeded with PVA–ZnO nanocomposites, these seeded substrates are annealed at (a) 250 °C, (b) 350 °C, (c) 380 °C, (d) 450 °C, and (e) 550 °C.

3.4. TEM images

Fig. 7 shows typical transmission electron microscopy (TEM) images of the nanorods produced at the bottom of the beaker after washing with DI water several times and redistribution in ethanol solution. The images show the free-surface ZnO nanorods, as observed in the FESEM images. This nanorod powder is usable in other applications.

3.5. Photoluminescence measurements

The optical properties of as-grown nanorods and nanowires were determined at room temperature by photoluminescence (PL) spectroscopy, where the PL spectra of all samples were excited by a He–Cd laser (wavelength $\lambda = 325$ nm). Fig. 8 shows the PL spectra of nanorods/nanowires grown on p-type (1 1 1) silicon substrates for samples A–E. The dominant peaks observed in the UV region are attributed to the near band edge UV-emission (NBE) of the wide bandgap of ZnO, which results from the recombination of free excitons [48–50]. The strong and sharp UV emission peak intensity at small full width at half maximum (FWHM), as observed in the PL spectrums of the ZnO nanorods, is a unique characteristic of nanostructured materials [51]. In Fig. 8c, the UV peak of sample C contains a shoulder at the right side of the peak. This is to be expected due to surface excitons of small diameter nanorods. In addition, this shoulder seemed to respond to the various rod sizes, as observed in the FESEM image in Fig. 6f [52]. Furthermore, the weak visible peak centered at 530 nm (green emission) can be compared to the very high UV emission peak. The green emission in the visible region is related to oxygen vacancies, zinc vacancies [53], and other associated structural defects. The weak visible peak for samples C, D, and E shows that the prepared ZnO nanorods had few oxygen vacancies or structural defects. In addition, the peak appearing at ~760 nm was connected to interstitial oxygen, which occurred due to excess oxygen in the synthesized ZnO nanorods [54]. These ZnO nanorods exhibited a high-quality hexagonal structure, as con-

firmed by FESEM images and EDX measurements; however, the low number of oxygen vacancies and defects lead to high resistivity; they are responsible for carrier concentration in the ZnO lattice [48]. In addition, the intensity ratio of the UV peak to the visible peak (I_{UV}/I_{vis}) in the ZnO nanorods was ~175 at room temperature for samples C and E, compared to 66.4 in Ref. [55], 80 at room temperature in Ref. [56], and 560 at 83 K in Ref. [57]. This high ratio can serve as a benchmark for this study and is the optimum indicator of excellent crystal quality and good optical properties of the ZnO nanorods/nanowires [57–59].

3.6. Raman spectra

According to group theory, wurtzite ZnO material is from the C_{6v}^4 space group. At the Γ point of the Brillouin zone, the optical phonon modes consist of 1A1 + 2B1 + 1E1 + 2E2 modes [60]. The A1 and E1 are polar Raman active modes vibrating at different frequencies, where A1 is polarized along the *z* direction and E1 is polarized along the *x*–*y* plane. The two B1 modes are silent and the two E2 modes are Raman active. The E2 modes separate into two sub-modes: E2 (low) modes are associated with the vibration of the heavy Zn sublattice, while E2 (high) modes are associated with oxygen atoms [61]. The incident radiation of the backscattering geometry used to collect Raman scattering is perpendicular to the *c*-axis of the ZnO nanorods; therefore, the Raman selection rules allow only modes E2 (high) and A1 (LO) [62]. The values of E2 (high) mode for samples A and B, as shown in Fig. 9 (a and b), respectively, appear at 437.8 nm, while for samples C, D, and E they appear at 436.7 nm, 437.3 nm and 436.7 nm, respectively. This peak is a unique property of the Raman active mode of wurtzite hexagonal ZnO and is very sensitive to strain of this material [55,63]. As a result, the red shift of the value of E_2 (high) with respect to the bulk value (437 nm) for samples A and B represent the tensile strain and the blue shift with for bulk value for samples C, D, and E represent the compression strain [64]. This result is consistent with the results obtained by X-ray diffraction (relation (6)). The highest value of the E_2 (high) peak for sample E compared to other samples indicates good quality and crystallinity of the ZnO nanorods in this sample [65]. Thus, the type and crystallinity of the structure can be predicted from the Raman spectra [66]. Finally the peaks located at 302 nm and 521 nm in Fig. 9 come from the silicon substrate.

4. Conclusions

Vertically aligned ZnO nanorods perpendicular to the substrate surface were grown using a seed layer consisting of ZnO nanocrystals and PVA carbon grids. The annealing temperature of the seed layer played an important role in controlling the diameter of the ZnO nanorods. In addition, microwave-assisted heating of CBD provided excellent temperature distribution, leading to homogeneous nanorods growth in the absence of a temperature gradient. The vertically aligned nanorods exhibited a high-quality wurtzite crystal structure and excellent UV emission at room temperature.

Acknowledgements

The authors gratefully acknowledge support from a research university (RU) grant and University Sains Malaysia.

References

[1] J. Mou, W. Zhang, J. Fan, H. Deng, W. Chen, J. Alloys Compd. 509 (2011) 961–965.
[2] D.P. Singh, Sci. Adv. Mater. 2 (2010) 245–272.
[3] H. Morkoc, Ü. Özgür, Zinc Oxide Fundamentals, Materials and Device Technology, Wiley-VCH Verlag GmbH & Co. KGaA, Weinheim, 2009.
[4] A. Kaushal, D. Kaur, J. Alloys Compd. 509 (2011) 200–205.
[5] C. Zhang, F. Zhang, T. Xia, N. Kumar, J.-i. Hahm, Z.L. Wang, J. Xu, Opt. Express 17 (2009) 7893–7900.
[6] G.Z. Shen, D. Chen, Sci. Adv. Mater. 1 (2009) 213–226.
[7] T. Chen, S.Y. Liu, Q. Xie, Y.-L. Jiang, G.-P. Ru, R. Liu, X.-P. Qu, Microelectron. Eng. 87 (2010) 1483–1486.
[8] J. Chen, J. Li, J. Li, G. Xiao, X. Yang, J. Alloys Compd. 509 (2011) 740–743.
[9] Z. Zhang, X. Li, C. Wang, L. Wei, Y. Liu, C. Shao, J. Phys. Chem. C 113 (2009) 19397–19403.
[10] O. Lupan, V.V. Ursaki, G. Chai, L. Chow, G.A. Emelchenko, I.M. Tiginyanu, A.N. Gruzintsev, A.N. Redkin, Sens. Actuator B 144 (2010) 56–66.
[11] J.F. Conley, S. Lisa, O. Yoshi, Appl. Phys. Lett. 87 (2005) 223114–223116.
[12] S. Kumar, G.-H. Kim, K. Sreenivas, R. Tandon, J Electroceram. 22 (2009) 198–202.
[13] W. Wu, S. Bai, N. Cui, F. Ma, Z. Wei, Y. Qin, E. Xie, Sci. Adv. Mater. 2 (2010) 402–406.
[14] W.L. Hughes, Z.L. Wang, Appl. Phys. Lett. 82 (2003) 2886–2888.
[15] Y. He, J.-A. Wang, X.-B. Chen, W.-F. Zhang, X.-Y. Zeng, Q.-W. Gu, J Nanopart. Res. 12 (2010) 169–176.
[16] S.K. Sharma, A.I. Inamdar, H. Im, B.G. Kim, P.S. Patil, J. Alloys Compd. 509 (2011) 2127–2131.
[17] A.R. José, Synthesis, Properties, and Applications of Oxide Nanomaterial, John Wiley & Sons, New Jersey, 2007.
[18] T. Sagawa, S. Yoshikawa, H. Imahori, J. Phys. Chem. Lett. 1 (2010) 1020–1025.
[19] H. Yan, J. Wang, X. Zhong, J. Mater. Sci. Mater. Electron. (2010), doi:10 1007/s10854-010-0200-1.
[20] C. Periasamy, P. Chakrabarti, Sci. Adv. Mater. 3 (2011) 73–79.
[21] L. Feng, A. Liu, M. Liu, Y. Ma, J. Wei, B. Man, J. Alloys Compd. 492 (2010) 427–432.
[22] O. Lupan, T. Pauporte, B. Viana, I.M. Tiginyanu, V.V. Ursaki, R. Corte, ACS Appl. Mater. Interfaces 2 (2010) 2083–2090.
[23] H. Zeng, J. Cui, B. Cao, U. Gibson, Y. Bando, D. Golberg, Sci. Adv. Mater. 2 (2010) 336–358.
[24] S. Mahmud, J. Alloys Compd. 509 (2011) 4035–4040.
[25] O. Martínez, V. Hortelano, J. Jiménez, J.L. Plaza, S. deDios, J. Olvera, E. Diéguez, R. Fath, J.G. Lozano, T. Ben, D. González, J. Mass, J. Alloys Compd. (2011), doi:10.1016/j.jallcom.2011.02.063.
[26] K.M. McPeak, J.B. Baxter, Ind. Eng. Chem. Res. 48 (2009) 5954–5961.
[27] B. Cao, W. Cai, J. Phys. Chem. C 112 (2008) 680–685.
[28] S.A. Kamaruddin, K.-Y. Chan, M.Z. Sahdan, M. Rusop, H. Saim, J. Nanosci. Nanotechnol. 10 (2010) 5618–5622.
[29] R. Ding, J. Liu, J. Jiang, X. Ji, X. Li, F. Wu, X. Huang, Sci. Adv. Mater. 2 (2010) 396–401.
[30] S.K. Mohanta, D.C. Kim, B.H. Kong, H.K. Cho, W. Liu, S. Tripathy, Sci. Adv. Mater. 2 (2010) 64–68.
[31] E. Lai, W. Kim, P. Yang, Nano Res. 1 (2008) 123–128.
[32] K.-i. Ogata, H. Dobashi, K. Koike, S. Sasa, M. Inoue, M. Yano, Phys. Status Solidi C 7 (2010) 1592–1594.
[33] R.-C. Wang, H.-Y. Lin, S.-J. Chen, Y.-F. Lai, M. Huang, Appl. Phys. A 96 (2009) 775–781.
[34] P. Hyoungwon, B.K. Jae, Y.K. Yang, C.J. Yeon, L. Heon, Nanotechnology 21 (2010) 355304.
[35] A. Hu, F. Wu, J. Liu, J. Jiang, R. Ding, X. Li, C. Cheng, Z. Zhu, X. Huang, J. Alloys Compd. 507 (2010) 261–266.
[36] W. Sang, Y. Fang, J. Fan, Y. He, J. Min, Y. Qian, J. Cryst. Growth 299 (2007) 272–276.
[37] R.S. Kumar, R. Sathyamoorthy, P. Matheswaran, P. Sudhagar, Y.S. Kang, J. Alloys Compd. 506 (2010) 351–355.
[38] Y. Tao, M. Fu, A. Zhao, D. He, Y. Wang, J. Alloys Compd. 489 (2010) 99–102.
[39] G. Kenannkis, D. Vernardou, E. Koudoumas, N. Katsarakis, J. Cryst. Growth 311 (2009) 4799–4804.
[40] D.-S. Kang, H.S. Lee, S.K. Han, V. Srivastava, E.S. Babu, S.-K. Hong, M.-J. Kim, J.-H. Song, J.-H. Song, H. Kim, D. Kim, J. Alloys Compd. (2011), doi:10.1016/j.jallcom.2011.02.010.
[41] Z.-X. Yang, X. Du, W. Zhong, Y. -X. Yin, M. -H. Xu, C. Au, Y.-W. Du, J. Alloys Compd. 509 (2011) 3403–3408.
[42] Y. He, W.J. Sang, a. Wang, R. Wu, J. Min, J. Nanopart. Res. 7 (2005) 307–311.
[43] Q. Li, V. Kumar, Y. Li, H. Zhang, T.J. Marks, R.P.H. Chang, Chem. Mater. 17 (2005) 1001–1006.
[44] K. Yuan, X. Yin, J. Li, J. Wu, Y. Wang, F. Huang, J. Alloys Compd. 489 (2010) 694–699.
[45] H. Wang, C. Xie, D. Zeng, J. Cryst. Growth 277 (2005) 372–377.
[46] R. Wahab, Y.-S. Kim, D.-S. Lee, J.-M. Seo, H.-S. Shin, Sci. Adv. Mater. 2 (2010) 35–42.
[47] C.-Y. Tsay, K.-S. Fan, S.-H. Chen, C.-H. Tsai, J. Alloys Compd. 495 (2010) 126–130.
[48] C.-F. Yu, C.-W. Sung, S.-H. Chen, S.-J. Sun, Appl. Surf. Sci. 256 (2009) 792–796.
[49] A. Umar, B. Karunagaran, E.-K. Suh, Y.B. Hahn, Nanotechnology 17 (2006) 4072–4077.
[50] P.-K. Samanta, P.-R. Chaudhuri, Sci. Adv. Mater. 3 (2011) 107–112.
[51] V.A. Fonoberov, K.A. Alim, A.A. Balandin, F. Xiu, J. Liu, Phys. Rev. B 73 (2006) 165317.
[52] Z.W. Liua, C.K. Ong, T. Yu, Z.X. Shen, Appl. Phys. Lett. 88 (2006) 053110.
[53] O.D. Jayakumar, V. Sudarsan, C. Sudakar, R. Naik, R.K. Vatsa, A.K. Tyagi, Scripta Mater. 62 (2010) 662–665.
[54] M. Willander, O. Nur, J.R. Sadaf, M.I. Qadir, S. Zaman, A. Zainelabdin, N. Bano, I. Hussain, Materials 3 (2010) 2643–2667.
[55] S. Wei, J. Lian, H. Wu, Mater. Charact. 61 (2010) 1239–1244.
[56] S.K. Mohanta, S. Tripathy, X.H. Zhang, D.C. Kim, C.B. Soh, A.M. Yong, W. Liu, H.K. Cho, Appl. Phys. Lett. 94 (2009) 041901–041903.

[57] D. Fan, R. Zhang, X. Wang, Solid State Commun. 150 (2010) 824–827.
[58] C. Sheng, O. Mario, Y. Zheng, K. Jieying, L. Jianlin, Appl. Phys. Lett. 93 (2008) 181106–181108.
[59] H.Q. Le, S. Tripathy, S.J. Chua, Appl. Phys. Lett. 92 (2008) 141910–141913.
[60] C.A. Arguello, D.L. Rousseau, S.P.S. Porto, Phys. Rev. 181 (1969) 1351–1363.
[61] R. Zhang, P.-G. Yin, N. Wang, L. Guo, Solid State Sci. 11 (2009) 865–869.
[62] F. Decremps, J.-P. Porres, A.M. Saitta, J.-C. Chervin, A. Polian, Phys. Rev. B 65 (2002) 092101.
[63] Q. Li, J. Bian, J. Sun, J. Wang, Y. Luo, K. Sun, D. Yu, Appl. Surf. Sci. 256 (2010) 1698–1702.
[64] C. Wang, Z. Chen, Y. He, L. Li, D. Zhang, Mater Sci.– Poland 28 (2010) 153–161.
[65] A. Khan, S.N. Khan, W.M. Jadwisienczak, Sci. Adv. Mater. 2 (2010) 572–577.
[66] A.-J. Cheng, Y. Tzeng, H. Xu, S. Alur, Y. Wang, M. Park, T.-h. Wu, C. Shannon, D.-J. Kim, D. Wang, J. Appl. Phys. 105 (2009) 073104.